Carbide coating on nickel to enhance the stability of supported metal nanoclusters†

Valeria Chesnyak, ‡[a,b] Srdjan Stavrić, ‡[a,c] Mirco Panighel, [a,b] Maria Peressi *[a] and Cristina Africh *[b]
Giovanni Comelli, [b]

The influence on the growth of cobalt (Co)-based nanostructures of a surface carbide (Ni_2C) layer formed at the Ni(100) surface is revealed *via* complementary scanning tunneling microscopy (STM) measurements and first-principles calculations. On clean Ni(100) below 200 °C in the sub-monolayer regime, Co forms randomly distributed two-dimensional (2D) islands, while on Ni_2C it grows in the direction perpendicular to the surface as well, thus forming two-atomic-layers high islands. We present a simple yet powerful model that explains the different Co growth modes for the two surfaces. A jagged step decoration, not visible on stepped Ni(100), is present on Ni_2C. This contrasting behavior on Ni_2C is explained by the sharp differences in the mobility of Co atoms for the two cases. By increasing the temperature, Co dissolution is activated with almost no remaining Co at 250 °C on Ni(100) and Co islands still visible on the Ni_2C surface up to 300 °C. The higher thermal stability of Co above the Ni_2C surface is rationalized by *ab initio* calcu-lations, which also suggest the existence of a vacancy-assisted mechanism for Co dissolution in Ni(100). The methodology presented in this paper, combining systematically STM measurements with first-prin-ciples calculations and computational modelling, opens the way to controlled engineering of bimetallic surfaces with tailored properties.

1 Introduction

During the last two decades, cobalt (Co) nanostructures have been investigated in light of various possible applications ranging from magnetic storage devices to heterogeneous catalysis. The smallest systems in nature that exhibit catalytic properties – single-atom catalysts (SACs) – clearly demonstrate how important is the choice of the support, since it determines the activity, selectivity and stability of adatoms and therefore the efficiency of SACs.[1–3] Among many possible other metals, SACs very often involve Co atoms due to their potential for hydrogen evolution, oxygen reduction, and hydrodeoxygenation reactions.[4–7] Climbing up the size scale from single Co adatoms to nanoclusters, it is worth noting that the interaction with the substrate determines also the size and shape of the aggregates, that, in turn, determine their properties.[8–12]

In the present study, we chose nickel (Ni) as supporting surface for Co nanoclusters because it allows to compare easily the behavior on purely metallic and carbide surfaces. However, it is important to avoid the mixing of the two metallic species, typically happening when Co is deposited on bare Ni surfaces at elevated temperatures.[13,14] Keeping the Co nanoclusters stable on the highly interacting Ni surface upon annealing is thus a challenging task. Furthermore, when using Ni surfaces, the presence of contaminants, in particular C, can hardly be avoided[15] and can affect the structure of deposited Co.[16] In addition, contamination can lead to striking structural changes of the surface itself. In the case of Ni, high concentration of dissolved near-surface carbon leads to "clock" reconstruction of the surface, forming a nickel-carbide (Ni_2C) layer.[17–19] This appears to be an ideal model system for investigating how a controlled modification of the substrate can affect the structure and stability of the adsorbed Co nanostructures. Moreover, metal carbides are worth investigating on their own merits, as they present excellent catalytic activity in various reactions, from ammonia synthesis to hydroprocessing.[20,21] In particular, they share with Co clusters

[a]*Physics Department, University of Trieste, via A. Valerio 2, Trieste 34127, Italy. E-mail: peressi@units.it*
[b]*CNR-IOM, Laboratorio TASC, S.S. 14 Km 163.5, Basovizza, Trieste, 34149, Italy. E-mail: africh@iom.cnr.it*
[c]*Vinča Institute of Nuclear Sciences – National Institute of the Republic of Serbia, University of Belgrade, P. O. Box 522, RS-11001 Belgrade, Serbia*
†Electronic supplementary information (ESI) available: Construction and application of a DFT-based model to estimate the binding energy of cobalt nanostructures on Ni(100) and Ni_2C substrates. Additional stick-and-ball models for: other Co nanostructures on surfaces, Co adatoms at stepped surfaces; first step of dissolution process of Co on surfaces. Additional STM images for: step decoration; time evolution of Co nanostructures on Ni(100) and Ni_2C surfaces. See DOI: 10.1039/d1nr06485a
‡These authors contributed equally to this work.

an enhanced catalytic activity towards the hydrogen evolution reaction,[22] thus making the investigation of Co deposited on Ni_2C remarkably relevant.

In this work, a detailed investigation of the structural properties and growth of Co clusters deposited on a Ni(100) surface – both clean and covered by a single Ni_2C layer – by means of variable temperature scanning tunneling microscopy (STM) measurements and first-principle calculations is presented. The different observed nanostructures are firstly structurally characterized and then investigated towards their thermal stability. We found that, compared to bare Ni(100), the presence of surface Ni_2C slows down the dissolution of Co into the Ni bulk, thus enhancing the stability of Co clusters on the surface. Co diffusion barriers and the energetics of its aggregates are estimated on the basis of first principle calculations. A novel, simple energy model based on few parameters calculated by first principles from small clusters is proposed to estimate the relative stability of clusters of any size and predict their growth mode. Finally, on the basis of STM images acquired in real time during annealing and further first-principles calculations, a model for Ni-vacancy assisted Co dissolution process is suggested. The energy model and the methodology employed in this work are rather general and can be extended to other bimetallic adsorbate-surface systems of potential interest.

2 Experimental details

Sample preparation and STM measurements were carried out in a UHV chamber with a base pressure of 1×10^{-10} mbar. A Ni(100) crystal was cleaned, for each preparation, by at least three cycles of sputtering (10–20 min, 4 μA, 1 keV, $p_{Ar^+} = 2 \times 10^{-6}$ mbar) and annealing (10 min, 600 °C). At the end of this procedure, once the sample is back to room temperature (RT), the Ni(100) surface is mostly covered by a Ni_2C layer formed with C atoms present in the crystal bulk as contaminants and segregating towards the surface when annealed around 500 °C.[18] Conversely, in order to prepare a bare Ni(100) surface, the sample was only flashed to maximum 400 °C after sputtering, thus preventing C segregation and formation of Ni_2C, as confirmed by the absence of the 2×2 pattern, characteristic of the Ni_2C reconstruction, in the low energy electron diffraction (LEED) measurements. Co was evaporated by means of an electron beam evaporator (flux about 0.003 ML per min) yielding a nominal Co coverage of 0.1 monolayer (ML) after 30 min, as estimated from the STM images. STM measurements were performed in constant current mode with an Omicron variable-temperature scanning tunneling microscope (VT-STM) operated with a R9plus controller (RHK Technology). For the measurements of the temperature-induced Co dissolution, the sample was annealed directly in the STM stage at about 1 K s^{-1} and stabilized at the desired temperature for about 5 min before proceeding with the measurements. The STM images were processed by means of the Gwyddion software.[23]

3 Computational details

First-principles calculations were carried out in the framework of spin-polarized density functional theory (DFT) method using the Quantum ESPRESSO package, based on plane waves and pseudopotentials.[24,25] Exchange and correlation effects were taken into account within the generalized gradient approximation using the Perdew–Burke–Ernzerhof (GGA-PBE) parametrization form.[26] The electron wave functions and the electron density were expanded in plane waves basis sets with cutoff energies of 50 Ry and 300 Ry, respectively. The convergence threshold for total energy in self-consistent calculations was set to at least 1.0×10^{-9} Ry per atom. The calculated bulk Ni lattice constant is 3.52 Å, very close to the most widely accepted values in literature. The Ni(100) and Ni_2C/Ni(100) surfaces were modeled using 4×4 slabs in a tetragonal unit cell with four Ni layers in the first system and three Ni layers in the second. In cases when larger Co clusters on the surface were considered, 6×6 slabs were used instead of 4×4 so that the distance between the Co clusters from the neighboring images is larger than 6 Å. The thickness of the vacuum region along the *z*-axis was set to 15 Å at least. Increasing this value modified the total energies by less than 0.01 eV. The Brillouin zone of 4×4 and 6×6 slabs were sampled using the Monkhorst–Pack scheme[27] with (3,3,1) and (2,2,1) Γ-centered *k*-point grids, respectively, that correspond to the same *k*-point density and to three inequivalent *k* points in the irreducible wedge of the first Brillouin zone in both cases. All atoms but those from the bottom Ni layer were allowed to fully relax using the Broyden–Fletcher–Goldfarb–Shanno (BFGS) algorithm until all the forces' components were less than 0.001 Ry $Bohr^{-1}$ and the changes in total energy for two consecutive cycles not greater than 1.0×10^{-4} Ry.[28] Energy barriers for the diffusion processes of Co atoms were calculated employing the nudged elastic band (NEB) method and the quasi-Newton Broyden optimization scheme.[29,30] The Atomic Simulation Environment package was used for setting up the structures and for the visualization purposes during the computation.[31]

4 Results and discussion

To investigate the behavior of metallic Co on bare Ni(100) and on Ni_2C/Ni(100) (Ni_2C in the following), 0.1 ML of Co was evaporated on each substrate at RT and the corresponding surfaces were characterized by STM. Representative STM images of Co/Ni(100) and Co/Ni_2C are shown in Fig. 1 with line profiles taken along the solid lines on the STM images.

On the bare Ni(100) surface the terraces are partially covered by small, randomly distributed bright protrusions. Statistical analysis on several STM images indicates a characteristic height of ≈2.3 Å and a variable lateral size in the 5–30 Å range, as shown in the line profile (green) taken along five representative protrusions. These structures are readily assigned to one-atom-high Co islands, as depicted by the atomistic model in the inset of Fig. 1a. Although these two-

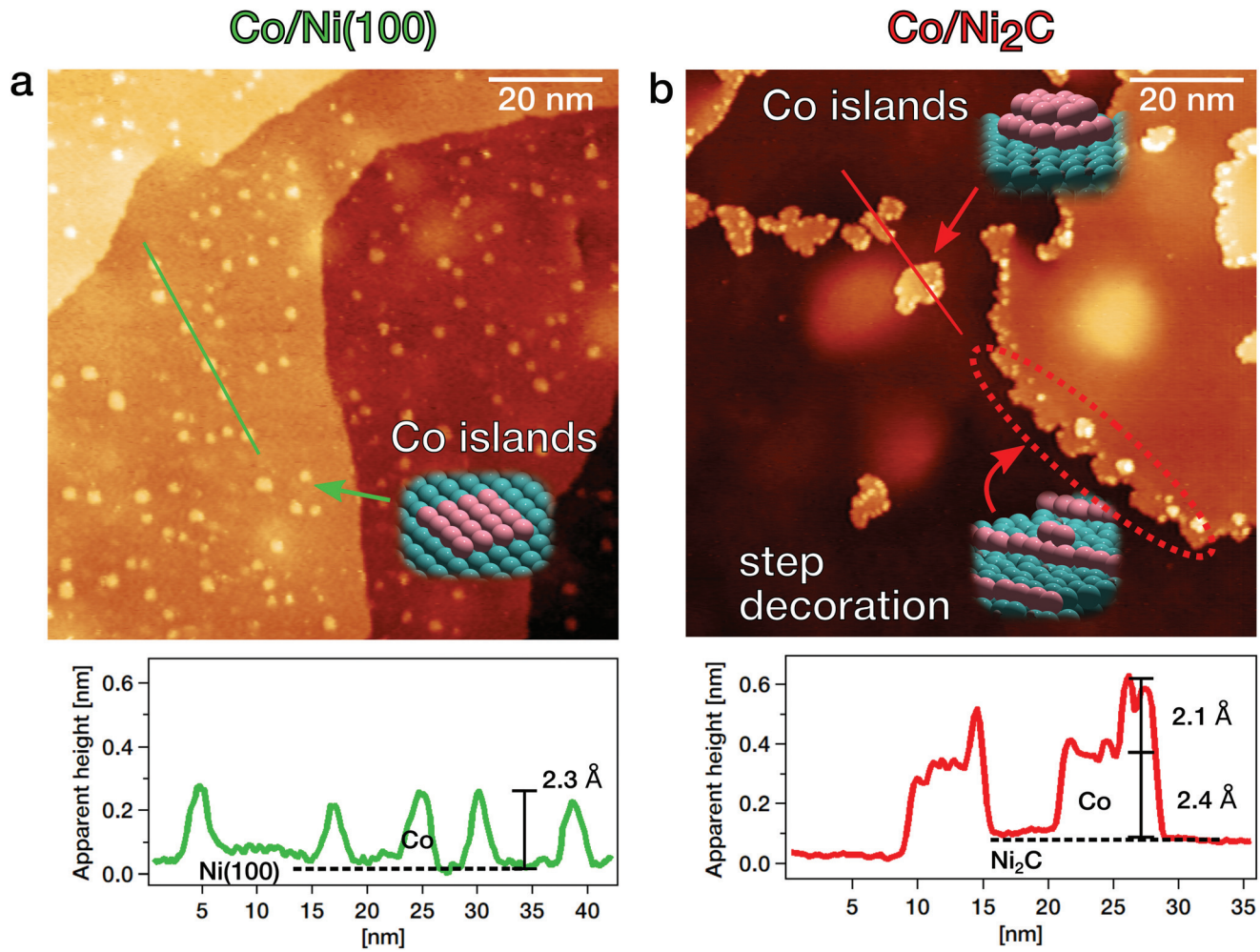

Fig. 1 Co nanostructures on Ni(100) (a) and Ni_2C (b) with corresponding line profiles (lower panels) taken along the solid lines in the STM images ((a) $V = -1$ V, $I = -2$ nA, (b) $V = -0.5$ V, $I = -0.8$ nA). On Ni(100), Co forms randomly distributed, one-atom high islands, as marked with the green arrow. On Ni_2C, larger, randomly shaped islands of Co, more than one-atom high, are growing. Besides, a step decoration along the Ni_2C edges, encircled in red, is observed. The insets show atomistic models of the different Co structures observed on the surfaces.

dimensional (2D) islands are few nanometers apart and situated at random sites on the terraces, they appear to be quite uniformly shaped and of similar lateral size. This epitaxial, so-called layer-by-layer growth model of Co deposited on bare Ni (100) was already reported[32] and is typical for metal films deposited on single crystals. The smooth, 5–10 nm wide spots in the baseline of the terraces for both bare Ni(100) and Ni_2C are most likely a consequence of the cleaning procedure, which can leave gaseous Ar encapsulated beneath the first few surface layers.[33]

On the Ni_2C-covered surface, fewer yet wider islands of more irregular shape are clearly visible. The abundance of these islands, also assigned to Co, is lower than on Ni(100), thus leaving the Ni_2C surface more exposed, while the line profile shown below Fig. 1b indicates a significant increase in their height. Unlike the Co islands formed on Ni(100), which are clearly 2D, Co islands deposited on the Ni_2C surface are more than one atomic layer high. This indicates the occurrence of three-dimensional (3D) growth, also known as Volmer–Weber, as depicted in the upper inset of Fig. 1b. The given apparent heights have again been obtained by averaging among several STM images. Another clear difference with Co on bare Ni(100) is that for Co on Ni_2C the steps of the surface always display a jagged shape and often appear to have additional brighter features on top. Especially at the boundary between the Ni_2C edge and the decoration, these additional adsorbates prefer to reside on top of the decoration rather than on the Ni_2C terrace. These features are tentatively assigned to Co atoms attached at the step edges, as illustrated in the bottom inset of Fig. 1b. This assignment will be confirmed in the following.

In order to explain the striking different behaviour of Co on Ni(100) and Ni_2C, we performed DFT calculations addressing the structural stability of Co adatoms and clusters (subsection 4.1) and the growth modes of larger Co nanostructures (subsection 4.2) on the two surfaces. In subsection 4.3 the step dec-

oration and the mobility of Co are discussed from both the experimental and theoretical points of view. Finally, subsection 4.4 addresses the thermal stability of Co nanostructures and their dissolution into the nickel bulk.

4.1 Structure and stability of small Co clusters on Ni(100) and Ni_2C surfaces

We firstly calculated the binding energy E_{bind} of small Co clusters on Ni(100) and Ni_2C from DFT total energies as follows:

$$E_{bind} = \frac{1}{n}(nE(Co) + E(S) - E(Co_n/S)), \quad (1)$$

where n is the number of Co atoms in the cluster, E(Co) is the total energy of a Co atom in the gas phase, E(S) is the total energy of the surface, namely Ni(100) or Ni_2C, and $E(Co_n/S)$ is the total energy of the cluster adsorbed on the surface. E_{bind} is an indicator of the stability of a particular Co nanostructure: higher values correspond to more stable structures.

On Ni(100), we considered three possible Co adsorption sites (see Fig. 2a): on top of a Ni atom (tNi), in the hollow site surrounded by four Ni atoms (a 4-fold coordinated site, which we shortly label 4f), and in the bridge site between the two Ni atoms (br).

The 4f site is by far the most stable for Co, with E_{bind} of 4.32 eV, much higher than for br and tNi sites (3.47 eV and 2.82 eV, respectively). Similarly, in the case of the Ni_2C surface, a single Co atom prefers the site with the highest coordination – the 5f site with three Ni and two C neighbors (Fig. 2b), where E_{bind} is 3.32 eV. Co on top of a C atom (tC site) is also stable, but with a lower E_{bind} (3.09 eV), while it is unstable in tNi, from which it relaxes towards the closest 5f site. It is worth noting that E_{bind} on Ni_2C is 1 eV lower than on bare Ni, indicating a much weaker Co-surface interaction in the former case.

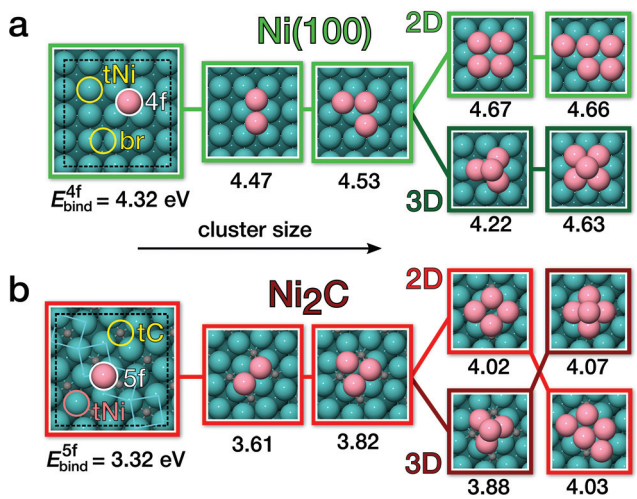

Fig. 2 Most stable adsorption configurations for Co adatom and small Co clusters on Ni(100) (green boxes) (a) and Ni_2C (red boxes) surfaces (b). The binding energy per Co atom is given in eV below each image. Lighter (darker) tone of frame color marks the 2D (3D) structure.

To examine the tendency of cobalt to cluster on Ni surfaces, we increase the number of Co atoms in the structures. Strong Co–Co attraction is already evident from Co dimers – the E_{bind} of Co_2 is 4.47 eV per atom and 3.61 eV per atom when adsorbed on Ni(100) and Ni_2C surfaces, respectively, an increase of 0.15 eV per atom and 0.29 eV per atom compared to a single Co atom. This is mainly due to the formation of a Co–Co bond, which is therefore stronger on Ni_2C than on Ni(100).

In order to obtain an initial guess about the preferred growth mode we examined the clusters with four and five atoms, which are the smallest nanostructures that can take both 2D and 3D shapes. On Ni(100), the squared Co_4 is much more stable than its tetrahedral counterpart, with a 0.45 eV per atom higher E_{bind} (Fig. 2a). This significant energy difference indicates that it is unfavorable for Co to abandon the square geometry of the Ni(100) surface during the growth. Conversely, the 2D and 3D structures of Co_5 cluster are very close in energy, with E_{bind} for a planar Co_5 only 0.03 eV per atom higher than for the pyramidal 3D configuration. In this case the small advantage of 2D structure is due to an additional metal–metal bond, as going from planar to pyramidal Co_5 would require to break four Co–Ni and one Co–Co in order to have four new Co–Co bonds.

Similarly, we examine the stability of Co_4 and Co_5 clusters on Ni_2C. While planar rhombic Co_4 is still more favorable than the tetrahedral Co_4 (Fig. 2b), the difference in E_{bind} is only 0.14 eV per atom. A further increase in cluster size introduces a twist in the preferred geometry, as the 3D Co_5 is more stable than the 2D one, with a difference of 0.04 eV per atom. Furthermore, from the inspection of the shape of planar Co_5 we derive an important conclusion – Co on Ni_2C ignores the geometry of the surface and takes a shape reminiscent of an hexagonal lattice. The difference in the 2D structure of Co aggregates on Ni(100) and Ni_2C thus appears to depend on the surface periodicity – the Ni(100) is a square lattice. This behavior of cobalt on Ni_2C surface will be examined in detail in subsection 4.2.

4.2 Growth of cobalt on the two surfaces

We extend the investigation of the stability of Co nanostructures on Ni(100) and Ni_2C to larger Co_n clusters, with n up to 26, but limiting to 2-layer structures when considering a 3D growth mode. When a cluster is adsorbed on the surface, not all its atoms contribute equally to the structural stability. In a 3D structure, the Co atoms of the first adlayer are in contact with the surface and bound to the Co atoms of the second adlayer that are, on the other hand, bound only to the Co atoms from the first adlayer. DFT calculations yield the total energy and therefore distinguish the most stable structure, but, to separate the contributions to the total energy by Co atoms with distinct coordination, an additional effort is required. In the following we present a simple model that effectively describes the two factors that are crucial for determining the growth mode of Co aggregates on each surface – namely the interaction between Co atoms and their binding to the surface.

The binding energy per atom of a Co cluster with n_1 atoms on the surface and n_2 atoms in the second adlayer can be approximately split into different contributions:

$$\tilde{E}_{\mathrm{bind}} = \frac{1}{n}(n_1 E_1 + n_2 E_2 + n_{\mathrm{b}} E_{\mathrm{b}}), \quad n = n_1 + n_2, \qquad (2)$$

where E_1 (E_2) is the energy associated with the bond each Co atom in the first (second) adlayer forms vertically with the underlying Ni (Co) atoms; n_{b} (E_{b}) is the number (energy) of first-neighboring planar Co–Co interaction, with E_{b} assumed to be constant for the two adlayers. Eqn (2), with the parameters E_1, E_2, E_{b} (Table 1) derived from full DFT calculations on a few small clusters, as explained in ESI,† allows the estimation of the binding energy of one or two atomic layers clusters of any size.

Fig. 3 shows the binding energies for 2D and 3D clusters containing up to 26 atoms obtained from full DFT calculations (E_{bind}, points) and from the model ($\tilde{E}_{\mathrm{bind}}$, dashed lines), together with some optimized structures. The binding energies plotted in Fig. 3 are listed in Table S1† and other optimized structures are shown in Fig. S1 and S2.†

Our model not only correctly predicts the most stable structure for a given number of Co atoms, but also provides a rationale for the 2D or 3D growth mode on the two surfaces.

Fig. 3 shows at a glance that 2D structures are more stable than 3D ones on Ni(100), although the difference reduces at increasing cluster size. According to the model, as a rule of thumb, the addition of a Co atom in the second adlayer should be more favorable than in the first adlayer, as $E_2 > E_1$. However, the first step for the conversion from 2D to 3D, *i.e.* the jump of a Co atom from the first to the second layer, is thermodynamically unfavorable since $E_2 < E_1 + E_{\mathrm{b}}$, *i.e.* the energy cost to break a bond in the first layer is not compensated by the energy gain in the second layer. Furthermore, NEB calculations to simulate the conversion of $Co_5^{2D} \rightarrow Co_5^{3D}$, as depicted in the inset in the upper part of Fig. 3, predict a very high barrier (2.55 eV) for a Co atom climbing from the first to the second layer, thus providing an additional kinetic argument in favor of 2D growth.

This conclusion agrees perfectly with the STM observations, which never showed two-layer-high cobalt structures on Ni (100). Additional adatoms landing on Ni(100) surface find the closest island to attach and stay in the first adlayer. Moreover, since the evaporation is uniform and with a stable flux, we always observed homogeneous distribution of Co islands of similar size on Ni(100). Formation of 3D clusters by a direct impingement of a Co adatom on top of an existing island is in practice rather unlikely, considering the experimental conditions of low Co coverage (0.1 ML) and flux.

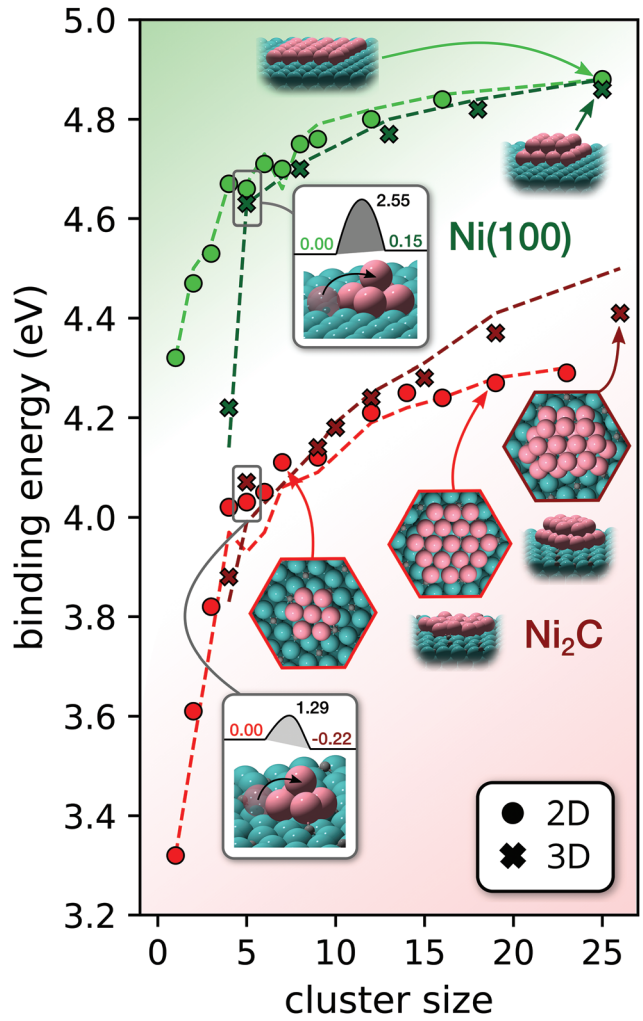

Fig. 3 Binding energy (E_{bind}) of 2D and 3D clusters on Ni(100) (green points) and Ni_2C (red points) from full DFT calculations. The prediction from the model ($\tilde{E}_{\mathrm{bind}}$) is represented with dashed lines. Some of the selected structures are depicted near the points that represent their binding energies. In the figure insets, total energy variations and barriers (in eV) for a Co atom to climb on top of the Co_4 clusters are presented for both the Ni(100) and Ni_2C surfaces.

Table 1 Parameters used in eqn (2) to estimate the binding energy of Co clusters on Ni(100) and Ni_2C surfaces

Substr.	E_1 (eV)	E_2 (eV)	E_{b} (eV)
Ni(100)	4.32	4.47	0.35
Ni_2C	3.32	4.04	0.43

On Ni_2C instead, Co shows a significant preference to arrange into 3D structures as the cluster size increases (Fig. 3). The stability order of the structures determined by DFT calculations is well reproduced by the model. By comparing the parameters in Table 1 for the two surfaces, it is evident that, on Ni_2C, binding in the second adlayer is more preferable than binding in the first, as E_2 is 0.72 eV higher than E_1, while the difference of those parameters on Ni(100) is only 0.15 eV. As the shape of larger Co clusters depicted in Fig. S2† clearly shows, Co on Ni_2C tends to recover its native crystal structure, arranging into two-layer-high lumps of hcp structure, thus displaying a behavior very similar to that of free Co clusters.[34,35] Once the small 2D hexagonal fragment of Co is built on Ni_2C,

Co atoms that arrive from the surface to the cluster jump above it and start building the second adlayer, where binding is more favorable. The $Co_5^{2D} \rightarrow Co_5^{3D}$ conversion through climbing of one Co atom, simulated with the NEB method and depicted in the inset in the lower part of Fig. 3, reveals in this case a barrier of only 1.29 eV on Ni_2C, *i.e.* about half of the value for the same process on Ni(100). From the model point of view, the addition of a first Co atom on top of a 2D Co cluster on Ni_2C has a positive energy balance with respect to its attachment to the first adlayer, as $E_2 > E_1 + E_b$. Further, once there is already at least one Co atom in the second adlayer, the addition to that adlayer becomes even more favorable, as broken Co–Co bonds in the first adlayer can be compensated with the bonds formed between Co atoms in the second adlayer. Putting together all the results presented in this paragraph, the preference of Co to form two-layer-high islands on Ni_2C finds a convincing explanation.

4.3 Mobility of Co and step decoration

Structural defects on surfaces, such as steps, kinks and vacancies, are low-coordination sites that typically exhibit higher activity for adsorption.[36,37] Despite the fact that steps are clearly visible in Fig. 1 on both Ni(100) and Ni_2C surfaces, they show a jagged appearance only in the latter case, which we attribute to Co decoration of the edges, yet another significant difference in Co adsorption on the two surfaces.

STM images of Ni(100) and Ni_2C steps, displayed in 3D to emphasize the different appearance of the edge, are shown in Fig. 4a and b, respectively. The corresponding line profiles taken along the green and red solid lines are extracted and reported in Fig. 4c. In the case of Ni(100), the step edge exhibits an apparent height of 2.3 Å, equivalent to one Ni(100) atomic layer. On the other hand, the step of Ni_2C is 0.2 Å higher at the edge, due to the chemical contrast of a decoration that runs all along the rim (arrow in the red line profile). Another representation of a decorated step is provided in Fig. S4† to emphasize the contrast. Above this Co decoration at the edge, the red line profile highlights the presence of an adsorbate 2.2 Å high, matching the height of a second Co adlayer. This feature will be discussed below.

To shed light on the presence of the Co step decoration on Ni_2C and its absence on Ni(100), we performed DFT calculations to examine the binding energy and the mobility of Co at the steps for the two surfaces. First, we find that, of all the possible sites in the steps vicinity, a single Co adatom prefers to bind at the foot of the step, with a binding energy of 4.73 eV and 4.31 eV on Ni(100) and Ni_2C, respectively (Fig. S3†). It is worth noting that these values are 0.41 eV and 0.99 eV higher than E_{bind} in the most favorable 4f and 5f sites at the respective surface terraces. However, our NEB calculations reveal that migration of a Co atom between adjacent 4f sites on Ni(100) surface terrace requires overcoming a barrier of 0.80 eV. This high diffusion barrier limits Co mobility and thus hinders Co decoration of the Ni(100) step edges despite the thermodynamic advantage of binding at the foot of the steps. A high energy barrier is also the likely explanation for the presence of only relatively small Co islands on the Ni(100) terraces in Fig. 1, as the formation of bigger islands requires cluster merging – a process that would be characterized by a much higher barrier than the migration of a single Co atom.

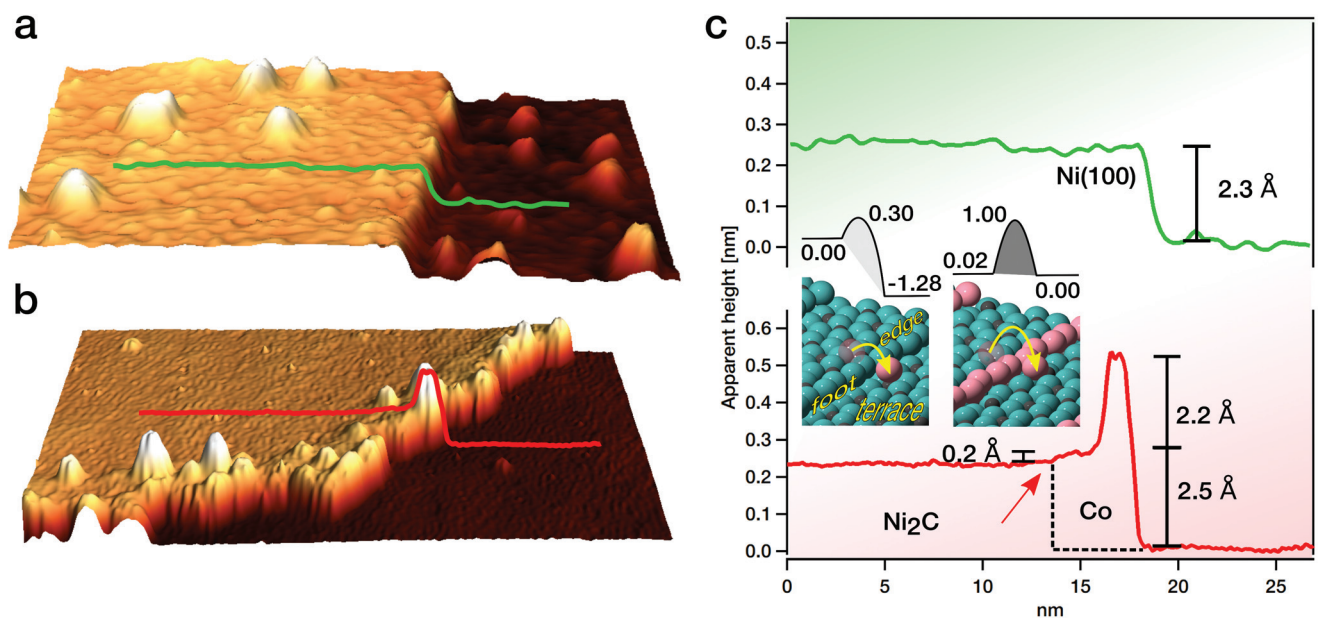

Fig. 4 STM images of Co/Ni(100) (a) and Co/Ni_2C (b), displayed in 3D ((a) $V = -1$ V, $I = -2$ nA, (b) $V = -0.5$ V, $I = -0.8$ nA). Line profiles along the green and red lines are reported in (c). In the case of Co/Ni(100), the step edge exhibits an apparent height of 2.3 Å, equivalent to one Ni(100) atomic layer, with no step decoration. In the case of Co on Ni_2C, the step is 0.2 Å higher at the edge, due to the chemical contrast of the Co decoration. Above this decoration a second Co adlayer 2.2 Å high is present. Energy variations and diffusion barriers (in eV) across the edge on Ni_2C are shown in the inset of (c).

Higher temperatures should allow Co to overcome these migration barriers, but would also activate a competitive dissolution process, as thoroughly explained in subsection 4.4 below.

On the Ni_2C surface, the calculated diffusion barrier for a Co atom is 0.42 eV, *i.e.* nearly halved with respect to the Ni (100) case. Therefore, Co atoms on Ni_2C can diffuse more easily across the terrace, until they attach to existing Co clusters, thus forming larger islands than on Ni(100), as indeed observed in the STM images (see Fig. 1b).

Alternatively, mobile Co adatoms on Ni_2C can reach a step edge and attach to it. If the step edge is downhill and made by Ni atoms only, the Co adatom can easily jump to the lower terrace where it finally rests at the foot of the step, as the barrier for this process is only 0.30 eV and the corresponding energy gain is 1.28 eV (left inset of Fig. 4c). Conversely, if the downhill step edge is already decorated by Co, jumping down is hindered since the barrier increases to 1.00 eV as a consequence of the stronger Co–Co bond with respect to Ni–Co and there is no energy gain in the final state (right inset of Fig. 4c). The Co atom is thus expected to remain at the top of the Co-decorated edge, as observed in the experimental images (red profile in Fig. 4b and c). Finally, if a Co adatom reaches a step foot, the uphill jump requires overcoming a barrier higher than 1 eV (1.58 eV in case of bare edge and 1.02 eV in case of Co-decorated edge, see again the insets of Fig. 4c). In conclusion, if a Co adatom reaches a Co-decorated edge, it sticks to it. Further diffusion along the edge is hindered, as the barrier for that process is 0.90 eV. The preference of Co to stick to the edges also explains the jagged appearance of the step decoration.

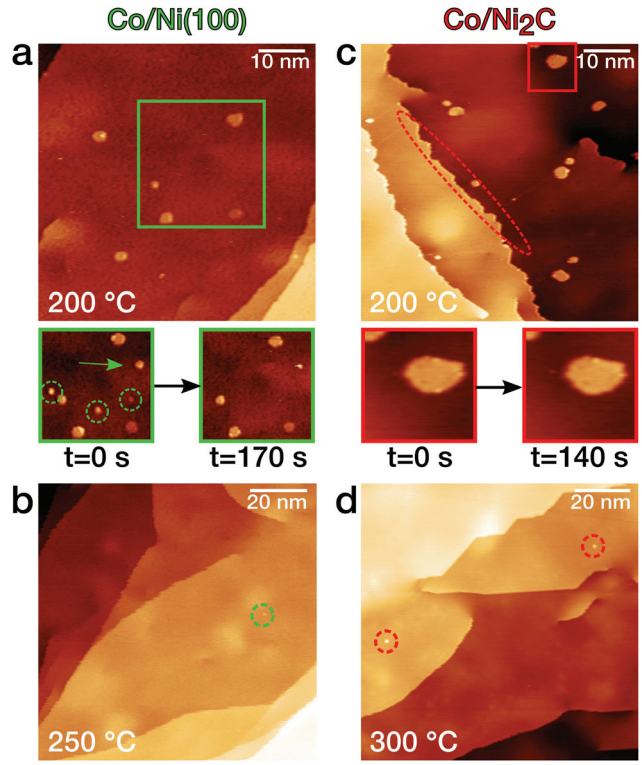

Fig. 5 Variable temperature STM images of Co/Ni(100) (a and b) and Co/Ni_2C (c and d) (a $V = -0.5$ V, $I = -1.4$ nA, b $V = -0.3$ V, $I = -1.4$ nA, c $V = -0.8$ V, $I = -1$ nA, d $V = -0.8$ V, $I = -0.4$ nA). Insets show the time evolution of islands within the same area scanned after 170 s (on Ni, $V = -0.5$ V, $I = -1.4$ nA) and 140 s (on Ni_2C $V = -0.8$ V, $I = -1$ nA). While on Ni the islands vanish or shrink after some scans, on Ni_2C they are more stable. The last traces of Co were seen at 250 °C on Ni and at 300 °C on Ni_2C, indicating a higher persistence of Co on Ni_2C.

4.4 Cobalt dissolution in nickel

The thermal stability of the Co clusters deposited at RT on both surfaces was investigated by acquiring STM images at elevated temperatures. The surface of Co/Ni(100) measured at 200 °C is shown in Fig. 5a. At this temperature Co islands are still clearly visible, but after a few minutes some of them disappear, as shown in the sequence of STM images in the green inset of Fig. 5a: after 170 s the highlighted islands vanish while the others shrink.

After further increase of the temperature to 250 °C, just a few, very small islands are still visible, as marked in Fig. 5b, while the surface appears elsewhere flat and clean, without other evidence of the presence of Co. A similar behaviour is reported for another bimetallic system, Ni on Pt: Ni dissolution into Pt bulk starts at ≈130 °C and is completed at ≈330 °C, when no Ni structures are observed by STM.[38]

At variance with Ni(100), in the case of Ni_2C at 200 °C the larger Co islands and the step decoration remain still clearly visible during scanning (Fig. 5c). Nevertheless, due to the increased mobility of Co, both the shape of the Co islands and the step decoration appear smoother than on the RT sample. Co dissolution is evidenced by STM after a few minutes, as highlighted in the red insets sequence shown in Fig. 5c, where the very same island does not change nor reduce after 140 s at 200 °C. More STM sequences of islands disgregation on the two surfaces can be found in Fig. S5(a and b on Ni(100), c and d on Ni_2C).†

Even at 300 °C some Co islands are still visible on Ni_2C, as shown in Fig. 5d. On the other hand, the steps do not exhibit a rough shape anymore and no chemical contrast is visible, indicating that at this temperature the Co step decoration has vanished. To summarize, contrary to the Co/Ni(100) case, the process of Co disappearance from the Ni_2C surface appears to be slower and occurs at higher temperatures. This can be rationalized by the stronger Co–Co bonding on Ni_2C that is responsible for the persistence of Co islands even at higher temperatures, although the mobility of Co, which is higher on Ni_2C than on Ni(100), could lead to a faster disgregation of the islands.

To better understand why Co does not prefer to stay on the Ni(100) surface upon annealing, we calculated the total energies of a Ni slab with a single substitutional Co atom either in the first, second or third layer from the Ni surface. The most stable configuration corresponds to Co in the second layer, while substitutions in the first and third layer are unfavored by 0.21 eV and 0.07 eV, respectively. The order is the same when a

full Ni layer is substituted with Co. The preference for substitutional Co atoms in the second layer can be ascribed to the advantage of maximizing the number of strong Co–Ni bonds while accommodating, thanks to surface elasticity, possible steric effects due to the substitution. The thermodynamic argument, clearly indicating the preference for Co in subsurface, therefore supports the experimentally observed trend for Co dissolution in the bulk. However, we do not claim that the most stable Co–Ni bimetallic structure is the one with a full Co ML in the second layer, as our DFT calculations are performed at $T = 0$ K and mixed structures typically form when the temperature is increased.[13]

In order to better understand the different behaviour of Co on Ni(100) and Ni_2C surfaces, we calculated the dissolution barriers into the bulk. We used the NEB method to simulate the replacement of a Ni atom from the first layer with a Co adatom (Fig. S6†). The barrier on Ni_2C is 0.74 eV higher than on Ni(100), revealing that such event is much more rare on Ni_2C. In this respect, Ni_2C acts as a protective layer against Co penetration, *i.e.* enhances the stability of Co on the surface. The same protective behavior of a tungsten carbide surface with respect to the bare Pt surface was reported for Ni dissolution.[39] To our knowledge, no direct comparison between a metal and its corresponding metal-carbide surface towards dissolution was yet reported, but a tendency of surface stabilization with increasing C amount in the cases of Mo and Ti carbides is indicated.[40]

The remaining question is how cobalt dissolution takes place. The simulation of such a complicated process goes beyond the scope of this article, but we can provide some hints. Previous studies report that bimetallic surfaces tend to mix through vacancies that segregate from the bulk to the subsurface and further to the surface.[41] Although vacancies are rather rare in metals, their presence in subsurface or bulk layers is energetically less favorable than at the surface, as a larger number of bonds needs to be broken. To quantify this statement for Ni(100), we simulated the segregation of a Ni-vacancy from the third to the second layer and then from the second layer to the surface. The first process involves a barrier of 0.96 eV, with a final state only slightly more stable than the initial one. In sharp contrast to this result, the barrier for the second process (second layer to surface) is only 0.29 eV, with a final state 0.83 eV lower in energy. We repeated the calculations replacing a Ni atom in the first layer, adjacent to a vacancy in the second layer, with a Co atom, thus simulating the vacancy-assisted dissolution of a single Co atom. The barrier for this process is only 0.20 eV, even lower than for the analogous process that does not involve Co, and the final state is 0.99 eV lower in energy than the initial one. It appears therefore that it is more favorable for the subsurface vacancy to be filled with a Co atom rather than with a Ni atom. This joint kinetic and thermodynamic argument is a clue that bimetallic systems, which contain both Ni-vacancies and Co atoms near the surface, will show tendency towards dissolution of Co as the vacancies gradually segregate.

5 Conclusions

Summarizing, a remarkable disparity in the growth mode of Co adsorbates on Ni(100) and Ni_2C surfaces is revealed by STM imaging and complementary DFT calculations. The surface Ni_2C layer that easily forms on Ni(100) upon segregation of C contaminants significantly weakens the Co-surface interaction and increases the strength of Co–Co attraction, thus favoring the growth of two-atomic-layer-high Co clusters. The weaker Co-substrate interaction on Ni_2C also leads to the formation of a decoration at steps, which is rationalized in terms of a lower diffusion barrier. A simple computational model, built upon DFT calculations performed on small Co clusters, is proposed in order to assess the binding energy for clusters of any size. The model can be used to predict the preferred arrangement of Co islands on any surface, also in cases hardly accessible to direct DFT calculations due to demanding computational efforts. Upon annealing, a competitive dissolution process sets in. This process is hampered when a Ni_2C layer is present, as confirmed by the calculated higher barrier for subsurface penetration. A few scenarios for Co dissolution into Ni(100) were considered, pointing towards a vacancy-assisted dissolution mechanism. In conclusion, our findings provide atomistic details of the processes occurring during deposition/annealing of Co on Ni, revealing that a Ni_2C coating enhances the stability of 3D clusters; our results open up new promising perspectives for engineering efficient catalysts. The proposed approach can easily be extended to other cases, as a way to tailor the catalytic properties of metal-supported nanocatalysts.

Author contributions

V. C. and S. S. equally contributed to the paper. M. Pa., V. C. and C. A. conceived the experiments. V. C. and M. Pa. performed the experiments and analyzed the experimental data. S. S. and M. Pe. conceived the simulations. S. S. performed and analyzed the simulations. All authors discussed the results. The manuscript was written through contributions of all authors. All authors have approved the final version of the manuscript.

Conflicts of interest

There are no conflicts to declare.

Acknowledgements

We acknowledge financial support from the Italian Ministry of Foreign Affairs and International Cooperation (Executive Programme with Serbia 2019–2021 – "Progetti di Grande Rilevanza"). This work has been also supported by the MIUR Progetti di Ricerca di Rilevante Interesse Nazionale (PRIN) Bando 2017 programme – grant no. 2017KFY7XF "FERMAT –

Fast ElectRon dynamics in novel hybrid organic-2D MATerials" and grant no. 2017NYPHN8 "MADAM – Metal Activated 2D cArbon-based platforMs". Computational resources have been obtained from CINECA through the ISCRA initiative and the agreement with the University of Trieste. We thank our colleague Pierre Thibault from the University of Trieste for his careful reading of the manuscript.

Notes and references

1 B. Qiao, A. Wang, X. Yang, L. F. Allard, Z. Jiang, Y. Cui, J. Liu, J. Li and T. Zhang, *Nat. Chem.*, 2011, **3**, 634–641.
2 Y. Chen, S. Ji, C. Chen, Q. Peng, D. Wang and Y. Li, *Joule*, 2018, **2**, 1242–1264.
3 P. Serp, *Nanoscale*, 2021, **13**, 5985–6004.
4 H. Fei, J. Dong, M. J. Arellano-Jiménez, G. Ye, N. D. Kim, E. L. Samuel, Z. Peng, Z. Zhu, F. Qin, J. Bao, *et al.*, *Nat. Commun.*, 2015, **6**, 1–8.
5 P. Yin, T. Yao, Y. Wu, L. Zheng, Y. Lin, W. Liu, H. Ju, J. Zhu, X. Hong, Z. Deng, G. Zhou, S. Wei and Y. Li, *Angew. Chem., Int. Ed.*, 2016, **55**, 10800–10805.
6 G. Liu, A. W. Robertson, M. M.-J. Li, W. C. Kuo, M. T. Darby, M. H. Muhieddine, Y.-C. Lin, K. Suenaga, M. Stamatakis, J. H. Warner, *et al.*, *Nat. Chem.*, 2017, **9**, 810–816.
7 A. Wang, J. Li and T. Zhang, *Nat. Rev. Chem.*, 2018, **2**, 65–81.
8 S.-R. Liu, H.-J. Zhai and L.-S. Wang, *Phys. Rev. B: Condens. Matter Mater. Phys.*, 2002, **65**, 113401.
9 M. J. Piotrowski, P. Piquini and J. L. F. Da Silva, *Phys. Rev. B: Condens. Matter Mater. Phys.*, 2010, **81**, 155446.
10 Y. Lu and W. Chen, *Chem. Soc. Rev.*, 2012, **41**, 3594–3623.
11 A. S. Chaves, M. J. Piotrowski and J. L. F. Da Silva, *Phys. Chem. Chem. Phys.*, 2017, **19**, 15484–15502.
12 Z. Xu, F.-S. Xiao, S. Purnell, O. Alexeev, S. Kawi, S. Deutsch and B. Gates, *Nature*, 1994, **372**, 346–348.
13 A. Christensen, A. V. Ruban, P. Stoltze, K. W. Jacobsen, H. L. Skriver, J. K. Nørskov and F. Besenbacher, *Phys. Rev. B: Condens. Matter Mater. Phys.*, 1997, **56**, 5822–5834.
14 A. V. Ruban, H. L. Skriver and J. K. Nørskov, *Phys. Rev. B: Condens. Matter Mater. Phys.*, 1999, **59**, 15990–16000.
15 C.-M. Sung and M.-F. Tai, *Int. J. Refract. Met. Hard Mater.*, 1997, **15**, 237–256.
16 S. W. Poon, J. S. Pan and E. S. Tok, *Phys. Chem. Chem. Phys.*, 2006, **8**, 3326–3334.
17 C. Klink, L. Olesen, F. Besenbacher, I. Stensgaard, E. Laegsgaard and N. D. Lang, *Phys. Rev. Lett.*, 1993, **71**, 4350–4353.
18 L. L. Patera, C. Africh, R. S. Weatherup, R. Blume, S. Bhardwaj, C. Castellarin-Cudia, A. Knop-Gericke, R. Schloegl, G. Comelli, S. Hofmann and C. Cepek, *ACS Nano*, 2013, **7**, 7901–7912.
19 C. Klink, I. Stensgaard, F. Besenbacher and E. Laegsgaard, *Surf. Sci.*, 1996, **360**, 171–179.
20 S. Oyama, *Catal. Today*, 1992, **15**, 179–200.
21 H. H. Hwu and J. G. Chen, *Chem. Rev.*, 2005, **105**, 185–212.
22 H. Zhang, X. Yang, H. Zhang, J. Ma, Z. Huang, J. Li and Y. Wang, *Chem. – Eur. J.*, 2021, **27**, 5074–5090.
23 D. Nečas and P. Klapetek, *Open Phys.*, 2012, **10**, 181–188.
24 P. Giannozzi, S. Baroni, N. Bonini, M. Calandra, R. Car, C. Cavazzoni, D. Ceresoli, G. L. Chiarotti, M. Cococcioni, I. Dabo, A. D. Corso, S. de Gironcoli, S. Fabris, G. Fratesi, R. Gebauer, U. Gerstmann, C. Gougoussis, A. Kokalj, M. Lazzeri, L. Martin-Samos, N. Marzari, F. Mauri, R. Mazzarello, S. Paolini, A. Pasquarello, L. Paulatto, C. Sbraccia, S. Scandolo, G. Sclauzero, A. P. Seitsonen, A. Smogunov, P. Umari and R. M. Wentzcovitch, *J. Phys.: Condens. Matter*, 2009, **21**, 395502.
25 P. Giannozzi, O. Andreussi, T. Brumme, O. Bunau, M. B. Nardelli, M. Calandra, R. Car, C. Cavazzoni, D. Ceresoli, M. Cococcioni, N. Colonna, I. Carnimeo, A. D. Corso, S. de Gironcoli, P. Delugas, R. A. DiStasio, A. Ferretti, A. Floris, G. Fratesi, G. Fugallo, R. Gebauer, U. Gerstmann, F. Giustino, T. Gorni, J. Jia, M. Kawamura, H.-Y. Ko, A. Kokalj, E. Küçükbenli, M. Lazzeri, M. Marsili, N. Marzari, F. Mauri, N. L. Nguyen, H.-V. Nguyen, A. O. de-la Roza, L. Paulatto, S. Poncé, D. Rocca, R. Sabatini, B. Santra, M. Schlipf, A. P. Seitsonen, A. Smogunov, I. Timrov, T. Thonhauser, P. Umari, N. Vast, X. Wu and S. Baroni, *J. Phys.: Condens. Matter*, 2017, **29**, 465901.
26 J. P. Perdew, K. Burke and M. Ernzerhof, *Phys. Rev. Lett.*, 1996, **77**, 3865–3868.
27 H. J. Monkhorst and J. D. Pack, *Phys. Rev. B: Solid State*, 1976, **13**, 5188–5192.
28 D. C. Liu and J. Nocedal, *Math. Program.*, 1989, **45**, 503–528.
29 G. Henkelman, B. P. Uberuaga and H. Jónsson, *J. Chem. Phys.*, 2000, **113**, 9901–9904.
30 G. Henkelman and H. Jónsson, *J. Chem. Phys.*, 2000, **113**, 9978–9985.
31 A. H. Larsen, J. J. Mortensen, J. Blomqvist, I. E. Castelli, R. Christensen, M. Dułak, J. Friis, M. N. Groves, B. Hammer, C. Hargus, E. D. Hermes, P. C. Jennings, P. B. Jensen, J. Kermode, J. R. Kitchin, E. L. Kolsbjerg, J. Kubal, K. Kaasbjerg, S. Lysgaard, J. B. Maronsson, T. Maxson, T. Olsen, L. Pastewka, A. Peterson, C. Rostgaard, J. Schiøtz, O. Schütt, M. Strange, K. S. Thygesen, T. Vegge, L. Vilhelmsen, M. Walter, Z. Zeng and K. W. Jacobsen, *J. Phys.: Condens. Matter*, 2017, **29**, 273002.
32 C. Egawa, H. Iwai and S. Oki, *Surf. Sci.*, 2000, **454–456**, 347–351.
33 M. Gsell, P. Jakob and D. Menzel, *Science*, 1998, **280**, 717–720.
34 C. D. Dong and X. G. Gong, *Phys. Rev. B: Condens. Matter Mater. Phys.*, 2008, **78**, 020409.
35 S. Datta, M. Kabir and T. Saha-Dasgupta, *Phys. Rev. B: Condens. Matter Mater. Phys.*, 2011, **84**, 075429.
36 B. Hammer, *Top. Catal.*, 2006, **37**, 3–16.
37 L. Vattuone, L. Savio and M. Rocca, *Surf. Sci. Rep.*, 2008, **63**, 101–168.

38 J. R. Kitchin, N. A. Khan, M. A. Barteau, J. G. Chen, B. Yakshinskiy and T. E. Madey, *Surf. Sci.*, 2003, **544**, 295–308.
39 T. G. Kelly and J. G. Chen, *Chem. Soc. Rev.*, 2012, **41**, 8021–8034.
40 P. Liu and J. A. Rodriguez, *J. Chem. Phys.*, 2004, **120**, 5414–5423.
41 D. Mahlberg and A. Groß, *ChemPhysChem*, 2021, **22**, 29–39.